PHYSICAL REVIEW D **80,** 125030 (2009)

Evolution and stability of cosmic string loops with Y-junctions

Neil Bevis,[1,*] Edmund J. Copeland,[2,†] Pierre-Yves Martin,[3,4,‡] Gustavo Niz,[2,§] Alkistis Pourtsidou,[2,‖] Paul M. Saffin,[2,¶] and D. A. Steer[3,**]

[1]*Theoretical Physics, Blackett Laboratory, Imperial College, Prince Consort Road, London, SW7 2BZ, United Kingdom*
[2]*School of Physics & Astronomy, University of Nottingham, University Park, Nottingham, NG7 2RD, United Kingdom*
[3]*APC, University Paris 7, 10, Rue Alice Domon et Léonie Duquet, 75205 Paris Cedex 13, France*
[4]*Glaizer Group, 32 rue Guy Moquet, 92240 Malakoff, France*
(Received 23 April 2009; published 29 December 2009)

We study the evolution of a particular class of nonperiodic cosmic string loops containing Y-junctions, such as may form during the evolution of a network of (p, q) cosmic superstrings. We set up and solve the Nambu-Goto equations of motion for a loop with junctions, focusing attention on a specific initially static and planar loop configuration. After a given time, the junctions collide and the Nambu-Goto description breaks down. We also study the same loop configuration in a $U(1) \times U(1)$ gauge field-theory model that allows composite vortices with corresponding Y-junctions. We show that the field-theory and Nambu-Goto evolution are remarkably similar until the collision time. However, in the field-theory evolution a new phenomenon occurs: the composite vortices can unzip, producing in the process new Y-junctions, whose separation may grow significantly, destabilizing the configuration. In particular, an initial loop with two Y-junctions may evolve to a configuration with six Y-junctions (all distinct from each other). Setting up this new configuration as an initial condition for Nambu-Goto strings, we solve for its evolution and establish conditions under which it is stable to the decay mode seen in the field-theory case. Remarkably, the condition closely matches that seen in the field-theory simulations, and is expressed in terms of simple parameters of the Nambu-Goto system. This implies that there is an easy way to understand the instability in terms of which region of parameter space leads to stable or unstable unzippings.

DOI: 10.1103/PhysRevD.80.125030 PACS numbers: 11.15.−q, 11.27.+d, 98.80.Cq

I. INTRODUCTION

Cosmic strings have long been known to arise in a wide class of field theories [1–4], and recent work has indicated that they may also arise in superstring/M-theory [5,6], for example, in models of brane inflation [7–9]. This has opened up the fascinating possibility that so-called cosmic superstrings, formed after a period of inflation, could provide a unique window on string theory, via measurements of their imprint on the cosmic microwave background radiation [10–15], their lensing of distant galaxies [16–18] or through their production of gravitational waves [19–21] and massive particles [22,23].

When two cosmic strings intersect, the traditional lore dictates that they intercommute (swap partners). For standard field-theory strings—essentially Abelian Higgs strings close to the Bogolmonyi limit—this intercommutation effectively occurs with unit probability [24–28]. However, for cosmic superstrings, the intercommutation probability is reduced due to the presence of extra dimensions and a small string coupling constant [29–32]. Furthermore, cosmic superstrings differ from conventional cosmic strings in that they come in different varieties: fundamental (F) strings, Dirchelet (D) strings, and also (p, q) composites of p F-strings and q D-strings. Composites split into their more basic elements at Y-shaped junctions, which are not present in the conventional cosmic string scenarios. This can lead to very different dynamics when strings collide, and a crucial outstanding question is how these Y-junctions affect the properties of the string network and its observational consequences.

However, this question is in fact not restricted to cosmic superstrings. Even the Abelian Higgs model can have stable composites and corresponding Y-junctions if the gauge coupling is set sufficiently high. Junctions are also generic in non-Abelian string networks. In this paper, we use the $U(1) \times U(1)$ model [33] to explore the properties of the Y-junctions it permits, focusing particularly on closed string loops with junctions. It should be noted, however, that the mass spectrum of bound states takes a specific form for cosmic superstrings, and this is not reproduced in the $U(1) \times U(1)$ model (or other field-theoretic models). As a consequence, some of the results presented in this paper will apply only to $U(1) \times U(1)$ strings, and cannot be extrapolated to the cosmic superstring case for which it is only a toy model. We will comment on this in more detail below.

The aim of this article is to compare two the different approaches which have so far been adopted to describe the

*n.bevis@imperial.ac.uk
†ed.copeland@nottingham.ac.uk
‡pym.aldebaran@gmail.com
§gustavo.niz@nottingham.ac.uk
‖ppxap1@nottingham.ac.uk
¶paul.saffin@nottingham.ac.uk
**steer@apc.univ-paris7.fr

dynamics of strings containing Y-junctions. The first, developed by Copeland, Kibble, and Steer (CKS) [34,35], is based on a modified Nambu-Goto action. The second considers strings as composite objects in terms of an underlying classical field theory, whose equations of motion can be solved for the string dynamics [33,36–43]. A similar comparison of the two approaches has a well established history for ordinary cosmic strings (with no Y-junctions), where it was shown that the Nambu-Goto action for a relativistic one-dimensional string is an excellent approximation to the dynamics of widely separated gauge cosmic strings—provided the curvature is on scales far greater than the microscopic string width (for a review see [2,3]). How does the comparison fare for strings with junctions, and particularly for closed loop configurations with junctions? Recently Bevis and Saffin [43] showed that the results obtained by CKS for the collision of straight strings are consistent with those found using field-theory simulations of the U(1) × U(1) model, once the composite region grows to be much larger than the string width. This is quite remarkable given the fact that the conditions for Nambu-Goto applicability are breached in the region of the Y-junction at all times (a related result was also shown for a different field-theory model in [44]).

In order to study loop configurations with junctions, we first extend the analysis of CKS to the multijunction case, and then solve the resulting equations numerically. In this way we can simulate the evolution of Nambu-Goto loops with junctions. We then compare their dynamics to field-theory dynamics of the same initial loop configuration.

If the Nambu-Goto evolution agrees well with the field-theory evolution, this is an important result since then further numerical simulations of the evolution of string networks with Y-junctions could be based on the Nambu-Goto equations, which are much less numerically costly than their field-theoretic counterparts. Furthermore, no known field-theory model yields the bound-state tension spectrum of cosmic superstrings, while in the Nambu-Goto case the tension of any string may be freely chosen. Additionally, the lowered intercommutation probability of cosmic superstrings may be trivially included in a Nambu-Goto simulation, since then intercommutation is dealt with by hand rather than being constrained by the dynamical equations as in the field-theory case.

For simplicity, in this paper we compare the field-theory and Nambu-Goto evolution of two initial loop configurations, which are variants of the butterfly-shaped string configuration shown in Fig. 1. While this loop resembles the result of two coplanar loops colliding, we stress that it is not intended to be representative of loops in a network. It merely presents an interesting case with which we may explore the properties of Y-junctions, including a new feature, their stability to decomposition into three separate Y-junctions.

In Sec. II, we discuss the Nambu-Goto approach and describe our numerical technique, for loops with just two junctions and also loops with multiple junctions. This is followed in Sec. III with a description of the field-theoretic simulations, and then in Sec. IV we present our results for each of the approaches including the identification of an instability in the field-theory case that is then seen for the first time to also be present in the Nambu-Goto case, once suitable initial conditions are chosen. We conclude in Sec. V and finish with some appendices giving derivations of some of the results used in the main paper, as well as technical details of our numerical codes.

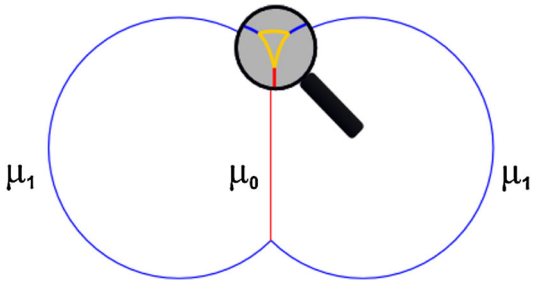

FIG. 1 (color online). An example of a loop configuration with multiple junctions: the butterfly configuration with a central string of tension μ_0 and two arc strings of tension μ_1. The basic butterfly configuration has just two junctions, but we find that under certain situations these can decompose, as indicated by the magnified region, with a single junction splitting into three junctions that then continue to separate.

II. NAMBU-GOTO APPROACH

As discussed in the introduction, CKS developed a formalism based on the Nambu-Goto action to study the dynamics of three semi-infinite strings meeting at a junction. In this section we outline the extension of this approach to configurations consisting of multiple interconnected junctions, such as that shown in Fig. 1, but the reader is directed to Appendix A for the full equations. We label the junctions with an index J.

Following CKS we form the total action of the system as the sum of the individual Nambu-Goto actions for each string plus terms containing Lagrange multipliers which constrain the strings to meet at the different junctions. Let the world sheet of the ith string be denoted by $x_i^\mu(t, \sigma_i)$. We work in Minkowski space-time, in the standard conformal-temporal gauge so that t is the background time and σ_i is the invariant length along the i-th string. Thus an element of string $d\sigma_i$ carries energy $\mu_i d\sigma_i$, with μ_i the string tension. The constraint equations are

$$\dot{\mathbf{x}}_i^2 + \mathbf{x}_i'^2 = 1, \tag{1}$$

$$\dot{\mathbf{x}}_i \cdot \mathbf{x}_i' = 0. \tag{2}$$

When three semi-infinite strings meet at a junction [34], one can always assign the coordinates σ_i such that they increase toward the junction on all three strings. However,

this is no longer possible when strings are connected to junctions at both ends. We therefore assign a parameter δ_i^J to the string ends, such that if σ_i increases along string i into junction J, then $\delta_i^J = +1$, while $\delta_i^J = -1$ if σ_i decreases into the junction. Note that if junctions J and K are connected by string i then $\delta_i^J = -\delta_i^K$.

This sign difference complicates slightly the governing equations, including the expression for energy conservation at the junction. As discussed in CKS, the rate of creation of one string at a junction must be balanced by the disappearance of one or both of the other strings that meet there. Let $s_i^J(t)$ be the value of σ_i at junction J, whose position is therefore

$$\mathbf{X}^J(t) = \mathbf{x}_i(t, s_i^J(t)) = \mathbf{x}_j(t, s_j^J(t)) = \mathbf{x}_k(t, s_k^J(t)), \quad (3)$$

where i, j, k are the indices of the three strings meeting at J. As a result the invariant length of string i created in time dt at this junction is $\delta_i^J \dot{s}_i^J(t)dt$. Then it can be seen that conservation of energy requires

$$\delta_i^J \mu_i \dot{s}_i^J + \delta_j^J \mu_j \dot{s}_j^J + \delta_k^J \mu_k \dot{s}_k^J = 0, \quad (4)$$

which is formally derived in Appendix A.

Another effect of the sign change relates to the identification of the waves along the string as ''incoming'' or ''outgoing'' from a junction. Away from any junction, the strings satisfy the usual wave equation

$$\ddot{\mathbf{x}}_i = \mathbf{x}_i'', \quad (5)$$

with general solution

$$\mathbf{x}_i(t, \sigma_i) = \tfrac{1}{2}[\mathbf{a}_i(u_i) + \mathbf{b}_i(v_i)], \quad (6)$$

where $u_i = \sigma_i + t$, $v_i = \sigma_i - t$ and the gauge conditions impose $|\mathbf{a}_i'| = |\mathbf{b}_i'| = 1$. While in CKS σ_i always increased towards the junctions and the incoming waves were always given by $\mathbf{b}_i$, in the multijunction case outgoing waves at junction J become incoming waves at the junctions to which it is connected. We shall discuss the difficulties related to this time-delayed coupling between junctions when we find solutions to the dynamical equations, but we must first generalize the CKS versions of those equations.

The equation for the time evolution of $\dot{s}_i^J$ as a function of the incoming waves (along strings i, j and k) at junction J becomes

$$1 - \delta_i^J \dot{s}_i^J(t) = \frac{\mu M_i[1 - c_i^J(t)]}{\mu_i \sum_h M_h[1 - c_h^J(t)]}, \quad (7)$$

where h takes values (i, j, k) and the incoming waves are combined via

$$c_i^J(t) = \mathbf{Z}_j \cdot \mathbf{Z}_k, \quad (8)$$

plus cyclic permutations, with

$$\mathbf{Z}_i = \begin{cases} +\mathbf{b}_i'(s_i - t) & \text{if } \delta_i^J = +1 \\ -\mathbf{a}_i'(s_i + t) & \text{if } \delta_i^J = -1. \end{cases} \quad (9)$$

Finally, we have the definitions: $\mu \equiv \mu_i + \mu_j + \mu_k$ and $M_i \equiv \mu_i^2 - (\mu_j - \mu_k)^2$, plus cyclic permutations. Note causality ($|\dot{\mathbf{X}}^J| \leq 1$) implies the triangle inequalities $M_j \geq 0$, as shown in [34].

We additionally find that the expression for the outgoing waves is

$$(1 + \delta_i^J \dot{s}_i^J)\mathbf{Y}_i = \mathbf{Z}_i(1 - \delta_i^J \dot{s}_i^J) - \frac{2}{\mu}\sum_h \mu_h(1 - \delta_h^J \dot{s}_h^J)\mathbf{Z}_h, \quad (10)$$

where again $h = (i, j, k)$ and also

$$\mathbf{Y}_i = \begin{cases} +\mathbf{a}_i'(s_i + t) & \text{if } \delta_i^J = +1 \\ -\mathbf{b}_i'(s_i - t) & \text{if } \delta_i^J = -1. \end{cases} \quad (11)$$

These then travel along the three strings and eventually reach the junctions to which J is connected.

Given an arbitrary initial configuration $(\mathbf{x}_i(0, \sigma_i), \dot{\mathbf{x}}_i(0, \sigma_i))$, we aim to solve for the full loop evolution and hence $(\mathbf{x}_i(t, \sigma_i), \dot{\mathbf{x}}_i(t, \sigma_i))$ for all $t > 0$. However, unless the configuration is highly symmetric, this calculation is analytically intractable, except at early times. Indeed, once an outgoing wave from one junction has reached another junction (or even returned to the same junction via a loop), then the incoming waves cannot be taken directly from the initial conditions and the problem becomes nonlinear. Useful analytical progress can be made for the two variants of our chosen initial conditions (see Fig. 1 and below), which we present in Appendices C and D, but for full solutions we employ numerical methods.

A. Numerical approach

We aim to follow the full evolution of relatively complex initial loop configurations for which, as discussed above, numerical methods are necessary. The procedure is the following: For every string i connecting two junctions, we work entirely with $\mathbf{a}'$ and $\mathbf{b}'$, reconstructing the closed string position $\mathbf{x}(t, \sigma_i)$ and velocity $\dot{\mathbf{x}}(t, \sigma_i)$ only a few times in the lifetime of the loop. The initial conditions fix $\mathbf{a}_i'(\sigma_i)$ and $\mathbf{b}_i'(\sigma_i)$ between all the junctions. First we calculate the $c_i^J(t = 0)$, from which $\dot{s}_i^J(t = 0)$ is determined using Eq. (7). Then at time δt, $s_i^J(\delta t)$, $u_i^J(\delta t)$ and $v_i^J(\delta t)$ can be calculated. The last step is to extend the domain of definition of $\mathbf{a}_i'(u)$ and $\mathbf{b}_i'(v)$, which can be done with Eq. (10). The time loop then continues.

Our simulation ends whenever the length of one string goes to zero, and hence when two junctions meet. The outcome of such a collision is not well understood for

cosmic superstrings, and in any case is not included in the Nambu-Goto description described above. However, the field-theory simulations discussed in Sec. III can of course continue beyond this time.

B. Initial conditions

We consider *two* closely related but different initial conditions.

The first is the butterfly configuration shown in Fig. 1, consisting of only two junctions (in other words, the small triangle shown in the magnifying glass is not present in this initial configuration). This planar loop consists of a straight string with tension μ_0 and two circular arcs with equal tensions μ_1. The strings are initially static: at the Y-junctions this imposes $\dot{s}_j = 0$ or equivalently that the vector sum of tensions at the junction J vanishes [see Appendix A, Eq. (A5)]

$$\sum_j \mu_j \delta_j^J \frac{\mathbf{x}_j'}{|\mathbf{x}_j'|} = 0. \tag{12}$$

Physically this corresponds to the fact that there can be no change in momentum occurring within a small volume surrounding the junction if the situation is static. Condition (12) imposes a relationship between the string tensions, the radius r of the two arcs making the butterfly ''wings'', and the distance x of their centers from the straight string

$$\frac{\mu_0}{2\mu_1} = \frac{x}{r} \equiv R. \tag{13}$$

The second initial condition is a modification of the first initial condition, in that we add, at each junction, the triangular shape shown in the magnifying glass in Fig. 1. Hence this initial configuration consists of 9 strings and 6 junctions, all of which are static. All the strings within the small triangles are given the same tension μ_2, and all are taken to be arcs of circles of size h, effectively the distance between the junctions. (The free parameter h will not affect the general physical behavior, if initially small. The use of arcs of circles is somewhat arbitrary but we believe that this choice does not have any dramatic effect on the local dynamics, since it is only the local curvature at $t = 0$ around a given junction that really affects its evolution. We will illustrate this in Sec. IV C, when studying the stability of Y-junctions).

The reason for considering this second initial condition is that our field-theory simulations of the simple butterfly configuration (with initially only two junctions) will show (see Sec. IV B) that the central straight string can be dynamically unstable into splitting, in a configuration very much like the one shown in Fig 1. As we discuss below, this phenomenon only occurs for specific U(1) × U(1) strings. However, this dynamical splitting cannot be accounted for in the Nambu-Goto equations, and hence we are forced to put it in by hand as an initial perturbation.

This point underlines the fact that the two types of simulation are rather different. Whereas the field theory is able to keep track of the topological windings of the vortices without external input, the Nambu-Goto strings know nothing of their composition, only their tension plays a role. Similarly, when two vortices interact in field theory, no external input is required. Nambu-Goto strings on the other hand do not know how to behave when they interact, and so boundary conditions must be added that preserve the topological windings of the vortices they are modelling. By allowing for triangular perturbations at the junctions, consistent with the topological demands of the field-theory vortices, we are explicitly allowing the Nambu-Goto strings to unpeel dynamically, in agreement with charge conservation. Another way to see this is to think of a Nambu-Goto string system as an evolving graph that, left to its own devices, does not change its connectivity—we need to add physical input to make such a system accurate.

III. FIELD-THEORETIC APPROACH

A. The field-theory model

While the Nambu-Goto formalism is relatively easy to analyze numerically, it does not necessarily give a complete description of Y-junctions—for instance, one might expect important interactions between the strings close to and at the junctions, and these are not included in the Nambu-Goto action. For that reason we also study the butterfly configuration using the U(1) × U(1) model of gauge strings [33], with Lagrangian density

$$\begin{aligned}\mathcal{L} = &-\frac{1}{4}F_{\mu\nu}F^{\mu\nu} - (D_\mu\phi)^*(D^\mu\phi) - \frac{\lambda_1}{4}(|\phi|^2 - \eta^2)^2 \\ &- \frac{1}{4}\mathcal{F}_{\mu\nu}\mathcal{F}^{\mu\nu} - (\mathcal{D}_\mu\psi)^*(\mathcal{D}^\mu\psi) \\ &- \frac{\lambda_2}{4}(|\psi|^2 - \nu^2)^2 + \kappa(|\phi|^2 - \eta^2)(|\psi|^2 - \nu^2).\end{aligned} \tag{14}$$

Here, we follow the conventions of [33,43] and

$$D_\mu\phi = \partial_\mu\phi - ieA_\mu\phi, \tag{15}$$

$$\mathcal{D}_\mu\psi = \partial_\mu\psi - igB_\mu\psi, \tag{16}$$

while the antisymmetric field strength tensors are given by

$$F_{\mu\nu} = \partial_\mu A_\nu - \partial_\nu A_\mu, \tag{17}$$

$$\mathcal{F}_{\mu\nu} = \partial_\mu B_\nu - \partial_\nu B_\mu. \tag{18}$$

Finally, η and ν are constants that set the energy-scales of the two halves of the model while λ_i and κ are dimensionless coupling constants.

For $\kappa = 0$ the two U(1)'s are uncoupled, and in the usual way each admits Nielsen-Olesen vortex solutions with

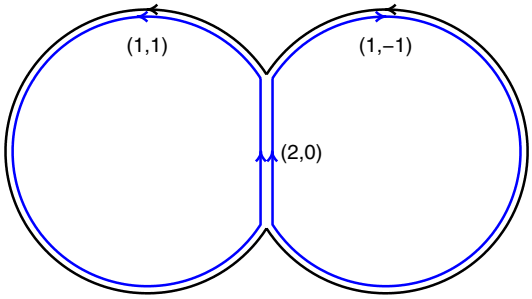

FIG. 2 (color online). The ϕ and ψ fluxes present in the butterfly configuration for field-theory simulations of case 2: $(1, 1) + (1, -1) \rightarrow (2, 0)$.

integer winding number. When $\kappa \neq 0$ the U(1)'s are coupled and, as shown in [33], for $0 < \kappa < \frac{1}{2}\sqrt{\lambda_1 \lambda_2}$, two parallel strings from each U(1) can bind reducing the potential energy of the system. Hence one can have Y-junctions in this theory and their formation as a result of the collision of two infinite straight strings was studied in Ref. [43], while cosmological networks have been studied in Ref. [41].

B. Numerical approach

The numerical approach employed for the field-theory simulations is largely that of Ref. [43], but with a very different set of initial conditions—namely the butterfly loop initial condition described above. The reader is referred to [43] for further details of the numerical code, while in Appendix B we discuss how to set up the initial conditions such as those given in Fig. 2.

IV. RESULTS

For both the Nambu-Goto and field-theory simulations, we have chosen to fix units such that the initial radius of the circular arcs is unity. Furthermore, for the field-theory simulations we take the standard [33,41,43] parameter choice $2 = \lambda_1 = \lambda_2 = 2e^2 = 2g^2$ and $0 < \kappa < 1$ in order for bound-states and Y-junctions to exist. We additionally set $\eta = \nu$ so that there is complete symmetry between the two halves of the model. Note that although the two Abelian Higgs models are each individually in the Bogomolnyi limit [45], with finite coupling between them, the ψ field affects the energy per unit length of a $(m, 0)$ string even though there is no winding in ψ and, for example, (2, 0) strings are stable (see Table I).

In the field-theory simulation, we have set up the butterfly initial configuration in two cases:

(i) *Case 1:* a (1, 0) and a (0, 1) string forming the "wings," with a (1, 1) bound-state string as the central segment (see Fig. 4 below).

(ii) *Case 2:* a (1, −1) and a (1, 1) string form the wings, so that a (2, 0) bound-state string forms the central segment (see Figs. 2 and 5)

TABLE I. The energy per unit length of an infinite static string, with parameters $\lambda_1 = \lambda_2 = 2e^2 = 2g^2 = 2$, $\eta = \nu$ and two values of κ as indicated. Note that an Abelian Higgs string of unit winding would yield $\mu = 2\pi\eta^2$ [45]. R is defined in Eq. (13).

κ	0.80	0.95
$\mu_{(1,0)}/2\pi\eta^2$	0.864	0.728
$\mu_{(1,1)}/2\pi\eta^2$	1.452	1.133
$\mu_{(2,0)}/2\pi\eta^2$	1.622	1.271
$R[(1, 0) + (0, 1) \rightarrow (1, 1)]$	0.840	0.778
$R[(1, 1) + (1, -1) \rightarrow (2, 0)]$	0.559	0.561

In the Nambu-Goto simulations (see Fig. 1) the tension of the wings is defined to be μ_1 while the tension of the central segment is μ_0. These therefore need to be chosen accordingly in order to compare with the field-theory results. Table I gives the string tensions for infinite straight strings (calculated via the method of [33]) for $\kappa = 0.8$ and 0.95.

From the definition of R in Eq.. (13), the relevant numerical values are also given in Table I and we see that, the smaller the value of R, the more stable the junction. In case 1, R is never very small since most of the energy actually stems from the covariant derivative term (which cannot be greatly reduced even by increasing κ to its maximum value). A large binding energy exists in case 2 since this involves flux cancellation. Indeed, for $\kappa = 0.95$, $R = 0.56$, meaning that a (2, 0) is only slightly heavier than a $(1, \pm 1)$ string.

A. Direct comparison of field theory and Nambu-Goto strings.

Before presenting our results it is useful to recall that a circular Nambu-Goto loop of unit radius collapses to a point in a time $\pi/2 \approx 1.57$. This is also the collapse time for those regions of the circular arcs on the butterfly wings that remain causally disconnected from the junctions.

For the initial condition given by case 1 with $\kappa = 0.8$, the Nambu-Goto results shown in Fig. 3 (left) reveal that the central bridge string collapses (and the junctions collide) at $t = 1.12 < \pi/2$. Although it is not shown here, for case 2 with $\kappa = 0.95$, the junctions collide later, at $t = 1.56 \lesssim \pi/2$. In the right panel of Fig. 3 we have taken $R = 0.5$ (and hence $\mu_0 = \mu_1$) for which the collapse time $\gtrsim \pi/2$. In this way we can show (magnified in the figure) the kink formed when parts of the arcs of circles in the butterfly wings instantaneously collapse to a point—at this time they travel at the speed of light. Something similar is also seen in the numerical simulations, but of course the field-theory vortices do not reach the speed of light.

A comparison of the field theory and Nambu-Goto results for case 1 with $\kappa = 0.8$ is shown in Fig. 4, while that for case 2 with $\kappa = 0.95$ is shown in Fig. 5. The snap shots

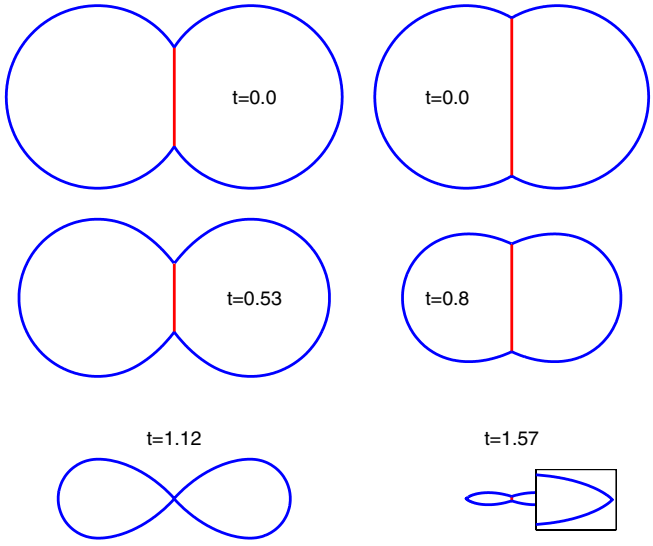

FIG. 3 (color online). Results using the Nambu-Goto method with tensions set to match a field-theory $(1,0)+(0,1)\rightarrow(1,1)$ case with $\kappa=0.8$ (left plot), and all tensions equal (right plot). The later case corresponds to $R=0.5$ and includes a magnified region showing a kink.

are at equal time intervals, and hence additionally show the velocity of the strings. The primary observation is that the agreement between the field-theoretic and Nambu-Goto results is excellent for the times shown, allowing us to extend the results from Ref. [43] to strings with global curvature rather than just straight strings with kinks, as was previously considered.

In order to make a more detailed comparison, we plot in Fig. 6 the physical length of the central bridge string as a function of time for both the Nambu-Goto and field-theory simulations. In the Nambu-Goto case, since this string is stationary, its length is simply given by the difference

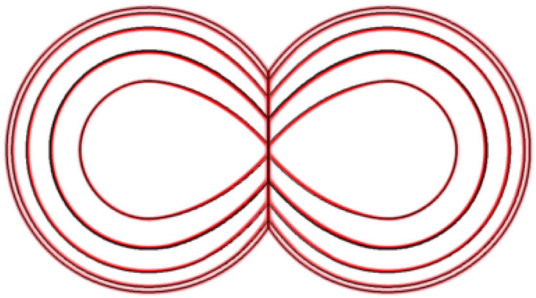

FIG. 4 (color online). The evolution of the butterfly configuration $(1,0)+(0,1)\rightarrow(1,1)$ with $\kappa=0.8$, shown at equally spaced time intervals: $t=0.000$, 0.267, 0.533, 0.800, 1.067, with larger configurations corresponding to earlier times. The field-theory solution is shown as a bitmap, representing the cumulative projection of its energy density onto the plane, while the Nambu-Goto solution is shown as a solid black line. The field-theory simulation had lattice spacing $\Delta x=0.5/\eta$, with $\eta=90$.

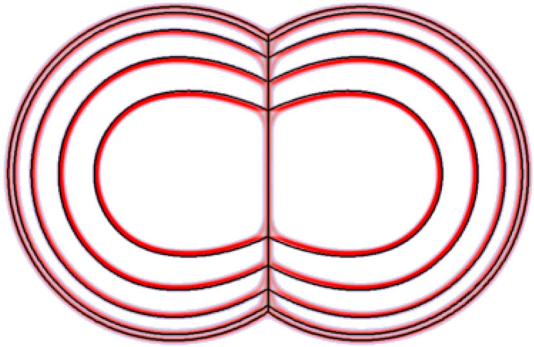

FIG. 5 (color online). As in Fig. 4 but for $\kappa=0.95$ and $(1,1)+(1,-1)\rightarrow(2,0)$.

between $s_0(t)$ at the two junctions and this value and this value can be obtained analytically, as in Appendix C, as well as being readily obtained from the simulations. In the field-theory case, the measurement of the string length is harder, though simplified because of the fact that the string always lies along the y axis. For example, in case 2 it is determined by the distance between the points where the path of the ψ winding cuts the y axis.

Our results again show excellent agreement between the Nambu-Goto and field-theoretic approaches, in fact right up to the moment of bridge collapse. There is a small initial transient departure, particularly in the $(1,1)+(1,-1)\rightarrow(2,0)$ case, but this is largely due to the initial conditions employed in the field-theory case, as well as the bridge

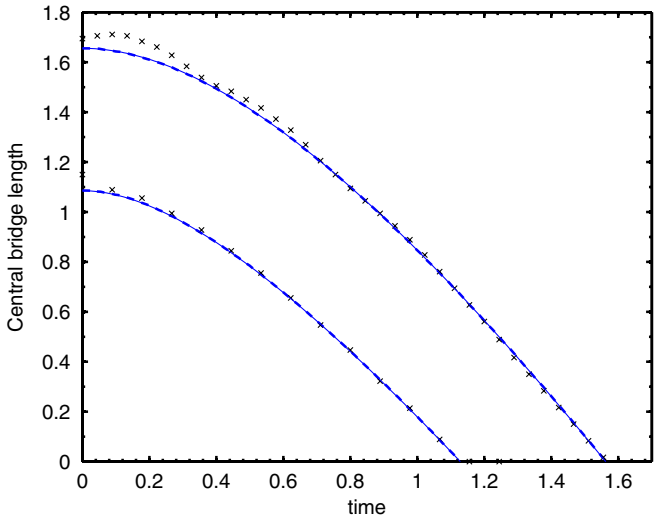

FIG. 6 (color online). The length of the central bridge string as a function of time for the analytic Nambu-Goto solution (thin), the numerical Nambu-Goto results (thick, dashed) and the field-theoretic results (crosses). The collection of data with lower bridge lengths is for the $(1,0)+(0,1)\rightarrow(1,1)$ case with $\kappa=0.8$ while higher bridge values correspond to $(1,1)+(1,-1)\rightarrow(2,0)$ with $\kappa=0.95$. The initial departure of the field-theoretic results from the Nambu-Goto ones is due to the measurement technique and is a transient effect.

length measurement technique (see Appendix C). The initial disagreement in Fig. 6 is just the (0, 1) string attempting to follow a smoother and less kinked route across the junction and therefore moving outwards from it, but then going too far and so undergoing a few low-level oscillations. These oscillations can been seen in Fig. 5, in which the two (1, 0) strings that compose the (2, 0) bridge separate slightly near the junctions.

B. Stability of Y-junctions to decomposition into multiple Y-junctions

When the initial butterfly configuration consists of the case 2 scenario of $(1, 1) + (1, -1) \rightarrow (2, 0)$, the field-theory simulation shows that the Y-junction itself can decompose as illustrated in Fig. 7. The reason this occurs is the following, and is specific to our U(1) × U(1) system: The central (2, 0) string is a bound state of (1, 1) and $(1, -1)$, but it can also be constructed from two (1, 0) strings. Whether this happens dynamically depends upon the string tensions and the orientations of the external strings. Let us define μ_2 to be the tension of the (1, 0) string and construct the following ratios:

$$R = \frac{\mu_0}{2\mu_1}, \qquad \mathcal{R} = \frac{\mu_1}{2\mu_2}. \tag{19}$$

For the range of κ chosen here $0.8 \leq \kappa \leq 0.95$, R is approximately constant at ≈ 0.56 (see Table I). On the other hand, $\mathcal{R}$ decreases from 0.86 to 0.78 as κ is increased across that range. As a result μ_2 becomes larger relative to both μ_0 and μ_1, which themselves stay in approximate proportion to each other. Hence, while case 2 with the high κ of 0.95, as already seen in Fig. 5, involves a large μ_2 and no decomposition, with a lower κ of 0.8 this decomposition does indeed occur and the outcome of the simulation is very different. In terms of ϕ and ψ windings, the central bridge string has peeled open to leave a system with two ϕ loops that sit at opposite ends of an elongated ψ loop, to which they are each bound.

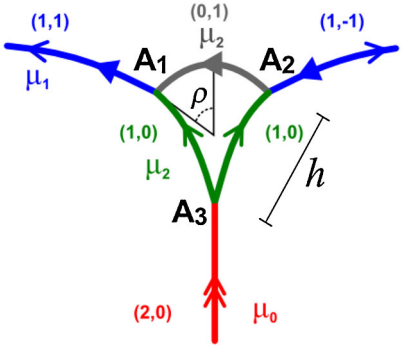

FIG. 7 (color online). In the field-theory, this diagram shows the possible decomposition of a $(1, 1) + (1, -1) \rightarrow (2, 0)$ junction into three separate Y-junctions. For the Nambu-Goto simulations this can be thought of as the second initial condition (magnified region of the butterfly configuration shown in Fig. 1), in which the Y-junction has split into three Y-junctions. In this case, the angles shown would be determined by the tensions, h, and the fact that the junctions are initially static.

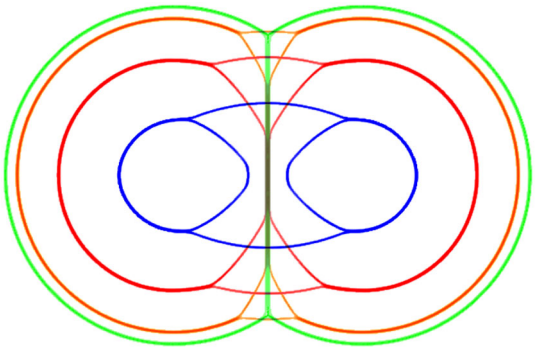

FIG. 8 (color online). Results from a field-theoretic simulation for $(1, 1) + (1, -1) \rightarrow (2, 0)$ with $\kappa = 0.8$, showing the decomposition of the initial Y-junctions. Snapshots are shown for times $t = 0$, 0.36, 0.8 and 1.24; each representing the cumulative projection of energy density on the plane. The simulation had lattice spacing $\Delta x = 0.5/\eta$, with $\eta = 90$.

Our results for $\kappa = 0.8$ are shown in Fig. 8; those for $\kappa = 0.95$ have already been presented in Fig. 5. In the former case the intermediate (1, 0) strings form and grow in the time-scale of the simulation. In the latter case, they form but do not grow in the time scale of the simulation. Indeed for $\kappa = 0.8$, the final state of the system is now very different: the central bridge has decomposed and peeled open to leave a system of two interconnected ϕ loops joined by ψ strings with four well-separated junctions.

Remarkably, we can also analyze this instability of the Y-junctions to decomposition in the Nambu-Goto picture, simply by changing the initial conditions and using the second initial condition described in Sec. II B. This is shown in Fig. 9 for the $\kappa = 0.8$ case (note though that the junctions are so close in the first subfigure that they cannot be resolved by eye). The snapshot for $t = 0.50$, however, clearly shows the new Y-junctions connected by circular arcs whose length increase with time. The matching with the field-theoretic results is surprisingly good. A similar Nambu-Goto evolution for $\kappa = 0.95$ now shows that the $(1, 1) + (1, -1) \rightarrow (2, 0)$ junction is *stable* to the breakup of junctions, again agreeing with the field-theory results. The precise numerical results do differ for the unstable case, since in the field-theoretic case there is a considerable role of the small-scale microphysics in the breakup of the junction and the breakup happens very much faster than is seen in the Nambu-Goto case. Additionally, the use of circular arcs here is artificial and would not be expected to be wholly accurate. However, the approximate matching of the critical value for κ at which the breakup occurs can be considered a success for the less computationally intensive CKS approach, and crucially, as we show below, it allows us to make a prediction based purely on the Nambu-Goto results as to when a junction

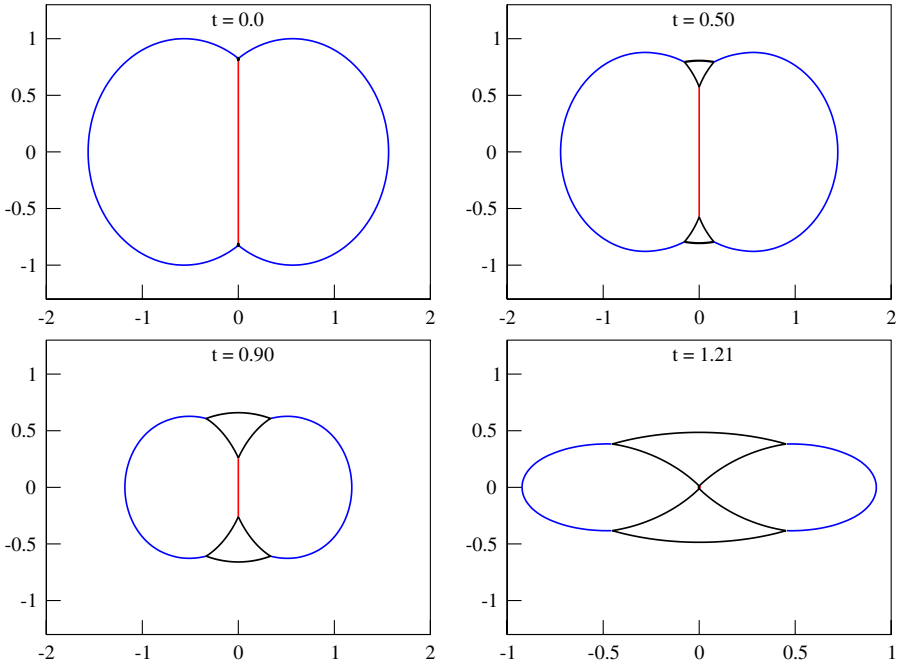

FIG. 9 (color online). Nambu-Goto evolution of the perturbed butterfly loop corresponding to the $\kappa = 0.8$ field-theory case of Fig. 8, using a perturbation parameter $h = 0.01$—the instability grows and the loop is unstable.

will and will not be unstable to decomposition into many junctions.

We reiterate that the Nambu-Goto string-junction system cannot change its connectivity if it simply follows the equations of motion. In order to model the physical system of vortices we must add physical input as to how the strings behave when they cross one another. Our approach has been to set up configurations that mimic the field-theory case just after the collision has occured. The nice result is that given an initial setup we then appear to be able to say with confidence what the outcome of the evolution will be, in that the prediction from the Nambu-Goto case matches closely the actual field-theory simulation.

C. Stability of Y-junctions in the Nambu-Goto approach

Using the Nambu-Goto approach, the stability of Y-junctions can be studied analytically, at least for small times. In Appendix D, we describe this procedure in detail for junction A_1 in Fig. 7. We find that the initial perturbation in the decomposed state grows or collapses according to the sign of the angle ρ (see Fig. 7) given by

$$\rho = \frac{\pi}{2} - \cos^{-1}(\mathcal{R}) - \cos^{-1}(R - h), \tag{20}$$

where h is the size of the initial perturbation. Therefore, for a given pair of tensions μ_0 and μ_1 there is a critical tension $\mu_2 = \mu_{\text{crit}}$ (for a small fixed h), for which $\rho = 0$. Below and above this critical limit, there are two distinctive behaviors: one in which the perturbation grows (as in Fig. 9) and one in which it either does not grow significantly or shrinks, and simply resembles the original butterfly (as in the field-theory simulation of Fig. 5). To illustrate this, we can use the analytic results for $\dot{s}_i$ and the evolution of the vertex $\mathbf{X}_{A_1}$ as a function of the right (and/or left movers), which explicitly is given by (see Appendix D)

$$\dot{\mathbf{X}}_{A_1} = -\frac{1}{\sum_j \mu_j} \sum_j \mu_j (1 - \dot{s}_j) \mathbf{b}'_j. \tag{21}$$

To map the junction movement in real space, it is useful to define the angle

$$\tan(\varphi) = \left(\frac{\dot{X}_y^{A_1}}{\dot{X}_x^{A_1}} \right), \tag{22}$$

which shows the direction with respect to the x axis for $t > 0$. The explicit treatment of this angle is given in Appendix D. The main result is that there exists a discontinuity in φ when going from $\rho > 0$ to $\rho < 0$, as Fig. 10 shows [46]. This shows how the evolution of the splitting of the Y-junction in the original butterfly depends mainly on the *initial local curvature* of the strings involved.

When $\rho > 0$ (see Fig. 7), strings 2 and 3 are "competing" in σ space while the butterfly wing (string 1) is not contributing much (note that for small times $\dot{s}_1 = 0$ to first order in t). After some time and in real space, the vertex A_1 moves downwards with an initial angle of $\varphi \geq \pi + \tan^{-1}(\sqrt{1 - R^2}/R)$ (with the equality in the limit of $\rho \to 0$) from the x axis, as can be seen in Fig. 10. In this case the perturbation does not grow and, for a tension μ_2 big enough, it may even collapse faster than the central

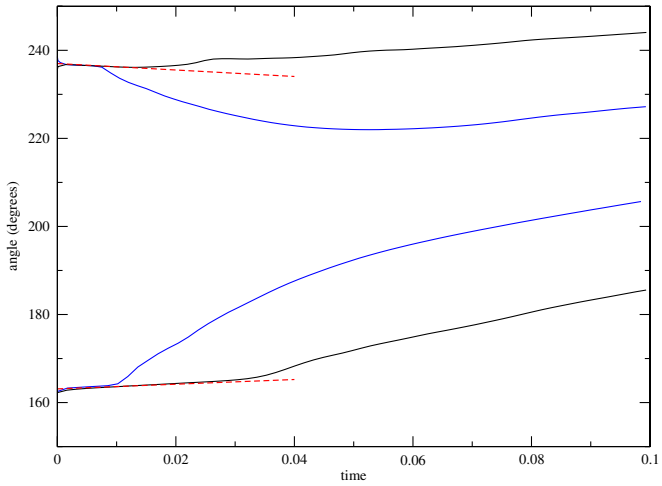

FIG. 10 (color online). Numerical (solid lines) and analytic (dashed red lines) evolution of the angle φ, for junction A1, for two cases with $\rho > 0$ and two with $\rho < 0$; all close to the critical value $\rho = 0$ (blue lines are closer to the critical value). For $\rho < 0$ (bottom curves) the Y-junction is said to be unstable, since vertex A moves along the butterfly wing until it reaches 180°, and then it starts moving towards the center of the big arc, as shown in Fig. 9. For $\rho > 0$ (top curves), vertex A moves downwards, leading to a stable Y-junction. The analytic approximations are calculated using $R = 0.561$ and Eqs. (D1) and (D12), which are linear truncations (in time), and only hold for small times since $\ell^{A_1}_{\rm min}(t) \sim h$. We choose $h = 0.01$.

bridge does. However, for $\rho < 0$ the local curvature is such that the strings of the triangular perturbation grow in σ space. In real space, vertex A_1 initially moves rapidly away from the y axis and almost along the butterfly wing (string 1), which corresponds to an initial angle of $\varphi \leq \pi - \tan^{-1}(R/(1-\sqrt{1-R^2})$ from the x axis. In Figs. 9 and 10, one can see this initial evolution. Later in the evolution (when the angle φ reaches π), the segment A_1A_2 changes from convex to concave, and the vertex A_1 evolves like any other point on the big arc segment, hence moving towards the center of the butterfly wing, as one can see in the last two plots of Fig. 9. Therefore, for $\rho < 0$ the perturbation grows for some time (which depends on how negative ρ initially is), implying the original butterfly Y-junction is unstable, leading to the criterion for stability based on simply obtaining the value for ρ.

V. DISCUSSION

The role of extended objects in the evolution of the Universe has been studied for many years owing to their intrinsically interesting properties, their crucial role in string/M-theory, repeated appearance in grand unified theory models and their presence in many condensed matter systems. Here, we have extended previous studies on the dynamics of cosmic strings to include the situations envisioned in models of cosmic superstrings, namely, the existence of bound-state strings, and the junctions that join them together [47]. While analytic studies of the superstrings themselves have met with limited success [29,30], the framework for numerical studies of field-theory defects is well developed, and simple models of bound-state strings [33] can be used to understand the large-scale properties of networks [38–41], as well as more detailed analyses on their individual collisions [43,44].

The great utility of Nambu-Goto dynamics is the huge reduction in the degrees of freedom compared to field-theory simulations, allowing for numerical computations with far larger dynamic range. However, as is well known, the Nambu-Goto dynamics break down as a description of gauged cosmic strings when two vortices cross, loops contract to a point, or when junctions collide. This is well established for the case of the usual Abelian cosmic strings, and algorithms have been developed (motivated by the field-theory results) which nevertheless allow the Nambu-Goto equations to be consistently used to model the evolution of a network of cosmic strings (see [3] for details). This same procedure has not yet been established for the case of strings with junctions, and has been a key goal of this paper. By comparing the modified Nambu-Goto equations for such strings, with the field-theory evolution for similar strings we have been able to establish how well they follow each other, and where differences emerge. By concentrating on a simple loop configuration, that nevertheless encapsulates important dynamics, we have been able to explore various properties and directly probe the relationship between these two approaches, answering questions such as: What happens when junctions collide? What is the effect of loop collapse on the wings of the butterfly loop? What can we say about the instability of junctions as the bound states try to unzip [42]?

In terms of the general dynamics, we have seen that the evolution of strings with junctions is remarkably well modeled by the Nambu-Goto action [34,35,48], despite the curvature at the junctions being high. However, the field-theory approach has opened up a crucial new instability that is not present in the usual Nambu-Goto formalism, namely, the breakup of a junction into three new junctions and the corresponding unzipping of the composite string. In other words we still need the field theory to understand the outcome of collisions of strings and collisions of junctions.

Examining the field theory of strings with different binding energies it became clear that for weakly-bound composites the junctions could cause the strings to unzip, care of the new instability. Once this was realized it became possible to model this within the Nambu-Goto dynamics by introducing the potentially unstable triangular configuration at the junctions, and solving for its evolution. Remarkably, this then allowed us to predict in terms of the angle ρ (or in terms of the string tensions) when a junction would be unstable to this decay mode, and when it would

remain stable, and the results agreed well with the field-theory simulations. With this done there is again excellent agreement between the Nambu-Goto simulations and the field theory. Of course have chosen a very specific string configuration to study, which is not representative of a cosmological network of cosmic superstrings. The key factor here is that given this understanding of the instability, we believe it will again be possible to perform, with confidence, large-scale cosmological simulations of cosmic superstrings using these modified Nambu-Goto strings, in the same manner that it is possible to perform simulations of ordinary cosmic strings using Nambu-Goto equations.

ACKNOWLEDGMENTS

We acknowledge financial support from the Royal Society (E. J. C.), STFC (N. B. and G. N.) and the University of Nottingham (A. P.). Field-theory simulations were performed on the UK National Cosmology Supercomputer (COSMOS) supported by SGI, Intel, HEFCE, and STFC. We would also like to thank T. Kibble for many useful discussions.

APPENDIX A: NAMBU-GOTO EQUATIONS OF MOTION

This appendix presents details of the results given in Sec. II. We work initially in the conformal gauge (and do not impose the temporal gauge) since this enables the equation for energy conservation to be obtained directly from the action. Denote the induced metric on the world sheet of the ith string by

$$\gamma^i_{ab} = \frac{\partial x^\mu_i}{\partial \sigma^a}\frac{\partial x^\nu_i}{\partial \sigma^b}\eta_{\mu\nu}, \tag{A1}$$

where $\sigma^0 = \tau$, $\sigma^1 = \sigma_i$ and $\eta_{\mu\nu}$ is the four-dimensional Minkowski metric. In the conformal gauge $\gamma^i_{00} = -\gamma^i_{11}$ and $\gamma^i_{01} = 0$, the action for the whole string configuration is

$$S = -\sum_i \Big[\mu_i \int d\tau \int d\sigma_i \sqrt{-x_i'^2\dot{x}_i^2}\prod_{J(i)}\Theta(\delta^J_i\{s^J_i(\tau) - \sigma_i\}) + \sum_{J(i)}\int d\tau f^{J,i}_\mu\{x^\mu_i(\tau, s^J_i(\tau)) - X^\mu_J(\tau)\}\Big],$$

where $J(i)$ implies that J takes on the values of the junctions at either end of string i (although for semi-infinite strings it would taken on just one value). The presence of the Θ terms ensures contributions only for the allowed range of σ values while the Lagrange multipliers $f^{J,i}_\mu$ ensure that the strings are coincident at the junction locations X^μ_J.

Varying the action with respect to X^μ_J for a single junction gives

$$\sum_{i(J)} f^{J,i}_\mu = 0, \tag{A2}$$

where now $i(J)$ implies that i takes on the indices of the strings that meet at junction J. Then, varying the action with respect x^μ_i for a single string yields, in general $\ddot{x}^\mu_i = x^{\mu\prime\prime}_i$ but at the junctions this becomes

$$\mu_i\delta^J_i(x^{\mu\prime}_i + \dot{s}^J_i\dot{x}^\mu_i) = f^\mu_{i,J}. \tag{A3}$$

We now set the more restrictive gauge condition $\gamma_{00} = 1$ (giving $\tau = t$ and σ as invariant length) while combining Eqs. (A2) and (A3). This yields immediately the energy conservation expression as the $\mu = 0$ equation

$$\delta^J_i\mu_i\dot{s}^J_i + \delta^J_j\mu_j\dot{s}^J_j + \delta^J_k\mu_k\dot{s}^J_k = 0, \tag{A4}$$

which is reproduced from the main text, and as there i, j, k are the indices of the three strings meeting at the junction.

In the new gauge and using the general solution of the wave equation, as in Eq. (6), the spatial equations become

$$\sum_{i(J)}\mu_i\delta^J_i[(1 + \dot{s}_i)\mathbf{a}'_i + (1 - \dot{s}_i)\mathbf{b}'_i] = 0. \tag{A5}$$

We then rewrite this using the new definitions of Eqs. (9) and (11) as

$$\sum_{i(J)}\mu_i[(1 + \delta^J_i\dot{s}_i)\mathbf{Y}_i + (1 - \delta^J_i\dot{s}_i)\mathbf{Z}_i] = 0. \tag{A6}$$

In addition the constraint that the three strings meet at the junction is

$$2\dot{\mathbf{X}}^J = (1 + \delta^J_i\dot{s}^J_i)\mathbf{Y}_i - (1 - \delta^J_i\dot{s}_i)\mathbf{Z}_i. \tag{A7}$$

Now eliminating the outgoing waves $\mathbf{Y}_i$ gives

$$\mu\dot{\mathbf{X}}^J = -\sum_{i(J)}\mu_i(1 - \delta^J_i\dot{s}^J_i)\mathbf{Z}_i. \tag{A8}$$

Furthermore, eliminating $\dot{\mathbf{X}}^J$ from Eqs. (A7) and (A8) we can solve for the unknown outgoing waves

$$(1 + \delta^J_i\dot{s}^J_i)\mathbf{Y}_i = \mathbf{Z}_i(1 - \delta^J_i\dot{s}^J_i) - \frac{2}{\mu}\sum_h\mu_h(1 - \delta^J_h\dot{s}^J_h)\mathbf{Z}_h,$$

which is reproduced from the main text. Squaring these equations and using the gauge condition that $|\mathbf{Y}_i| = |\mathbf{Z}_i| = 1$, then finally yields the result for $\dot{s}$ given in the main text as Eq. (7).

APPENDIX B: FIELD-THEORY INITIAL CONDITIONS

We obtain the initial conditions required for the butterfly configuration by first setting up the appropriate windings in the scalar field and then applying a period of dissipative evolution in order to relax the configuration to the minimum energy configuration. That is, during this period there is an extra term in each of the equations of motion that is proportional to the first time derivative of the correspond-

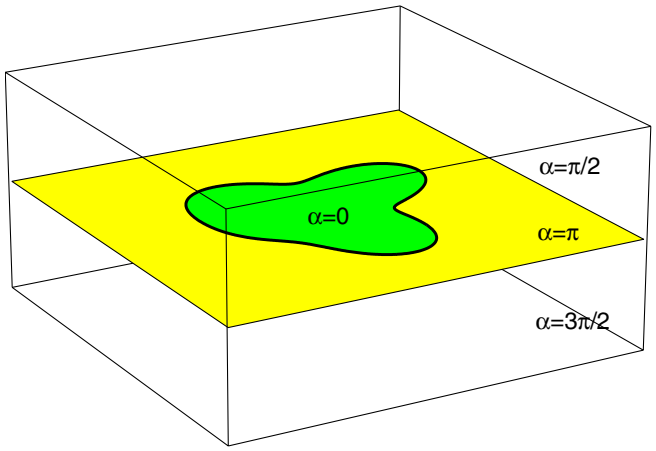

FIG. 11 (color online). The initial ϕ phase choice for a planar (1, 0) loop, ensuring a winding of 2π in the desired locations.

ing field and so removes energy from the system. Additionally, we fix the modulus of the scalar field in the region close to the desired center lines since otherwise the configuration would simply contract to a point during the dissipative evolution. We apply reflective boundary conditions throughout the simulation.

The initial choice for the phases of the ϕ field for a planar loop of (1, 0) string is made as shown in Fig. 11. If a site is above the plane of the loop then it is given the phase $\pi/2$, if it is below the plane then it is given $3\pi/2$, while if it is in the plane of the loop then it is given either π if it is outside the loop or zero if it is within it. This ensures the correct winding structure of the field but it obviously yields artificially high gradients on the plane of the loop. The modulus of the scalar field is initially chosen so that the field lies on the vacuum manifold, except close to the string center lines, as will be explained momentarily. During the dissipative evolution the gauge field, which is set to zero initially, quickly grows to counter these phases gradients, while the phase and modulus of ϕ rapidly adjust themselves in order to minimize the energy. Obtaining a (0, 1) loop can be achieved by simply swapping ψ for ϕ in the above argument, while a (1, 1) loop is obtained by setting up the phases appropriately in both fields. Higher winding numbers cannot be achieved by the direct application of the above approach and will be discussed below.

The modulus of the scalar fields is set inside a tube around the string centre line according to the solution for an infinite straight string. For a winding $2\pi m$ in the phase of ϕ and $2\pi n$ in the phase of ψ, this has the following form for small displacements r from the string center

$$\phi(r) \approx Cr^m, \tag{B1}$$

$$\psi(r) \approx Dr^n. \tag{B2}$$

The constants C and D, which depend on the choice of m and n cannot be found analytically, but are solved for using essentially the approach of Ref. [33]. Note that if m is finite but n is zero, then even though there is no winding in ψ, its modulus is still less than ν near the string as this lowers the total potential term energy. However, $|\psi|$ does remain finite as $r \to 0$. In principle we could fix $|\psi|$ close to the string in this case also, but we choose not to since it would not greatly aid the fixing of the string position and we wish to minimize the artificial restrictions enforced.

The butterfly configuration illustrated in Fig. 2 can be constructed by the superposition of a (1, 1) loop and a $(1, -1)$ loop after a period of dissipation. Since the equations of motion are nonlinear there is no precise means to do this, however a good approximation is simply to sum the gauge fields from each loop A_μ^+ and A_μ^- to give the total

$$A_\mu = A_\mu^+ + A_\mu^-, \tag{B3}$$

where the $+$ and $-$ refer to each loop. Then for the scalar fields

$$\frac{\phi}{\eta} = \frac{\phi_+}{\eta}\frac{\phi_-}{\eta} \tag{B4}$$

results in a superposition of complex phases [24,26,28,49]. Furthermore, at distances far from any string setup in ϕ_+ (such that the field is approximately constant and close to its vacuum) the form of ϕ is essentially that found in ϕ_-. Using these equations, the time derivatives must then superpose as

$$\partial_t A_\mu = \partial_t A_\mu^+ + \partial_t A_\mu^-, \tag{B5}$$

$$\eta \partial_t \phi = \phi_+ \partial_t \phi_- + \phi_- \partial_t \phi_+. \tag{B6}$$

While the wings are largely unaffected by this process and remain close to the minimum energy solution, a further period of dissipation is required to relax the central region, because of the significant interference between the two loops. For the case illustrated in Fig. 2 this includes the cancellation of the fluxes in ψ along the central string, which greatly reduces the energy per unit length of that segment.

APPENDIX C: ANALYTIC NAMBU-GOTO RESULT FOR THE BUTTERFLY CONFIGURATION WITH TWO VERTICES

As discussed in Sec. II, analytical progress is generally not possible once junctions become causally connected. However, in the case of the two-junction butterfly configuration, the symmetry present ensures that the central string is static and that it merely changes in length as time proceeds. This enables us to readily perform analytical calculations for this case that are valid in fact for all times of interest.

The initial conditions are a string lying on the y axis (string 0) and two arcs of unit circles (strings 1 and 2) in the x-y plane. If is useful to introduce an angle γ where, for a

static initial configuration, $\cos\gamma = -R = \mu_0/(2\mu_1)$. We then have

$$\begin{aligned}
&\mathbf{x}_0(t=0,\sigma_0) = (0,\sigma_0,0), \qquad |\sigma_0| < \sin\gamma,\\
&\mathbf{x}_1(t=0,\sigma_1) = (-\cos\gamma + \cos\sigma_1, \sin\sigma_1, 0), \qquad |\sigma_1| < \gamma,\\
&\mathbf{x}_2(t=0,\sigma_2) = (\cos\gamma - \cos\sigma_2, \sin\sigma_2, 0), \qquad |\sigma_2| < \gamma.
\end{aligned} \tag{C1}$$

If we label the lower vertex as A and the upper one as B, then σ_i increases toward junction B for all strings. Because of symmetry it is sufficient to study one junction, say B. Therefore, at $t = 0$

$$\begin{aligned}
&\mathbf{a}_0' = \mathbf{b}_0' = (0,1,0),\\
&\mathbf{a}_1' = \mathbf{b}_1' = (-\sin\sigma_1, \cos\sigma_1, 0),\\
&\mathbf{a}_2' = \mathbf{b}_2' = (\sin\sigma_2, \cos\sigma_2, 0).
\end{aligned} \tag{C2}$$

Conservation of energy (4) implies that $R\dot{s}_0^B = -\dot{s}_1^B$ and hence after integration we have

$$s_0^B(t) = \sin\gamma - \frac{1}{R}(s_1^B(t) - \gamma). \tag{C3}$$

Thus, it is sufficient to determine the function $s_1^B(t)$. In this case we have $c_1 = c_2 = \cos(s_1^B - t)$ and $c_0 = 2\cos^2(s_1^B - t) - 1$ and so it is useful to denote $\Delta = t - s_1^B$, whose derivative is $\dot{\Delta} = 1 - \dot{s}_1^B$. Therefore, Eq. (7) implies

$$\dot{\Delta} = \frac{1 - R^2}{1 + R\cos\Delta}. \tag{C4}$$

This simple separable equation can be integrated to give

$$t\sin^2\gamma = -\cos\gamma\sin\Delta + \Delta - \cos\gamma\sin\gamma + \gamma. \tag{C5}$$

Together with the definition of Δ and Eq. (C3), we now have t, s_0^B and s_1^B specified as functions of the variable Δ.

Ordinarily the above results, which rely on the incoming waves into the junctions taking the form specified by the initial conditions, would cease to be valid for times after the junctions come into causal contact. However, as noted above, the symmetry means that string 0 is always static. We therefore know trivially the waves emitted from the junctions along this string, which take the same form as in the initial conditions. Therefore, the above results are valid even after the junctions are in causal contact via this central route. Further, it can be shown that the central string always reaches zero length before communication is possible via the arcs. Hence, the above results are actually valid for all times of interest.

APPENDIX D: STABILITY OF Y-JUNCTIONS USING THE NAMBU-GOTO APPROXIMATION

As long as we restrict ourselves to early times, we can study the stability of the initial perturbation introduced in the butterfly configuration. We will consider junction A_1 (see Fig. 7), however this analysis can be equally applied to any other junction. The angles shown in Fig. 7 are completely determined by the initial equilibrium conditions and hence they are defined in terms of the tensions μ_1 and μ_2. The position of junction A_1 in σ space is

$$\begin{aligned}
s_1^{A_1}(0) &= \gamma = \pi - \cos^{-1}\left(\frac{\mu_0}{2\mu_1} - h\right),\\
s_2^{A_1}(0) &= \eta = \cos^{-1}\left(\frac{\mu_0}{2\mu_2}\right) - \alpha,\\
s_3^{A_1}(0) &= \rho = \gamma - \alpha - \frac{\pi}{2},
\end{aligned} \tag{D1}$$

where $\alpha = \cos^{-1}\frac{\mu_1}{2\mu_2}$ and h is the distance between junction A_1 (or A_2) and junction A_3 in Fig. 7.

We will now analytically demonstrate that the behavior of the perturbation (i.e. whether it grows or collapses) depends on whether the angle ρ is positive or negative. For that we will consider both cases and study the behavior of $\dot{s}_i^{A_1}$ and $\dot{\mathbf{X}}^{A_1}$. We will drop the junction index (A_1) from now on for simplicity.

Case I: $\rho < 0$

The initial configuration comprises of three strings with tensions μ_1, μ_2 and

$$\begin{aligned}
&\mathbf{b}_1'(t=0,\sigma_1) = (\sin\sigma_1, \cos\sigma_1, 0),\\
&\mathbf{b}_2'(t=0,\sigma_2) = (-\sin\sigma_2, \cos\sigma_2, 0),\\
&\mathbf{b}_3'(t=0,\sigma_3) = (-\cos\sigma_3, \sin\sigma_3, 0).
\end{aligned} \tag{D2}$$

At a later time t the incoming waves at junction A are

$$\begin{aligned}
&\mathbf{b}_1'(t, s_1(t)) = (\sin(s_1(t) - t), \cos(s_1(t) - t), 0),\\
&\mathbf{b}_2'(t, s_2(t)) = (-\sin(s_2(t) - t), \cos(s_2(t) - t), 0),\\
&\mathbf{b}_3'(t, s_3(t)) = (-\cos(s_3(t) - t), \sin(s_3(t) - t), 0).
\end{aligned} \tag{D3}$$

Taylor expanding s_i we get $s_i(t) = s_i(0) + \lambda_i t^2 + \ldots$ (remember $\dot{s}_i = 0$ initially), and using the relations between the angles we find (to first order in t)

$$\begin{aligned}
c_1 &= \cos(2\alpha + 2t),\\
c_2 &= -\cos\alpha,\\
c_3 &= -\cos(\alpha + 2t).
\end{aligned} \tag{D4}$$

Now, using Eq. (7), linearizing in t and defining $\mathcal{R} = \cos\alpha = \frac{\mu_1}{2\mu_2}$ (which is always less than unity due to the triangle inequalities) we find

$$\dot{s}_1 = -\dot{s}_3 = -\frac{1}{\sqrt{1 - \mathcal{R}^2}}t, \qquad \dot{s}_2 = \left(\frac{2\mathcal{R} - 1}{1 - \mathcal{R}^2}\right)t. \tag{D5}$$

Case II: $\rho > 0$

In this case, the initials conditions can be written as

$$\begin{aligned}
&\mathbf{b}_1'(t=0,\sigma_1) = (\sin\sigma_1, \cos\sigma_1, 0),\\
&\mathbf{b}_2'(t=0,\sigma_2) = (-\sin\sigma_2, \cos\sigma_2, 0),\\
&\mathbf{b}_3'(t=0,\sigma_3) = (-\cos\sigma_3, -\sin\sigma_3, 0).
\end{aligned} \tag{D6}$$

Following the same procedure we find

$$\dot{s}_1 = 0, \qquad \dot{s}_2 = -\dot{s}_3 = -\frac{2\sqrt{1-\mathcal{R}^2}}{1+\mathcal{R}}t. \tag{D7}$$

Having the analytic expressions for $\dot{s}_i$ (which of course can be extended further than first order in t) we can easily find the analytical expression for $\dot{\mathbf{X}}$ using Eqs. (A5) and (A7), to obtain the expression

$$\dot{\mathbf{X}} = -\frac{1}{\sum_j \mu_j}\sum_j \mu_j(1-\dot{s}_j)\mathbf{b}'_j. \tag{D8}$$

In order to study the motion of the vertex in real space, we define the angle

$$\tan(\varphi) = \left(\frac{\dot{X}_y}{\dot{X}_x}\right). \tag{D9}$$

Since the expression for this angle is very complicated, one can take the limit in which the perturbation size h tends to zero, and also consider small deviations from the $\rho = 0$ case, either with positive or negative ρ. The critical tension μ_2 which leads to $\rho = 0$ is obtained by setting (20) to zero and solving for μ_2, resulting in

$$\mu_{\text{crit}} = \frac{\mu_1}{2\cos(\cos^{-1}(R-h)-\pi/2)}. \tag{D10}$$

Therefore, in the limit $h \to 0$ and $\mu_2 = \mu_{\text{crit}}$ Eq. (D8) reduces to

$$\frac{\dot{X}_y}{\dot{X}_x} = -\frac{R}{1+\sqrt{1-R^2}} + \frac{-1+3R^2+\sqrt{1-R^2}}{R^2(1+\sqrt{1-R^2}-2R^2\sqrt{1-R^2})}t \tag{D11}$$

for $\rho < 0$, and

$$\frac{\dot{X}_y}{\dot{X}_x} = \frac{\sqrt{1-R^2}}{R} - \frac{2+R^2-2\sqrt{1-R^2}}{2R^4}t \tag{D12}$$

for $\rho > 0$. Notice that, as one should expect, in the critical tension limit $\mathcal{R}$ drops out from the expressions, and only $R = \frac{\mu_0}{2\mu_1}$ appears. For both cases ($\rho > 0$ and $\rho < 0$), $\dot{X}_x$ is initially positive, so it is the y direction which changes. For $\rho > 0$, the vertex A_1 moves with an initial angle of

$$\varphi = \pi + \tan^{-1}\left(\frac{\sqrt{1-R^2}}{R}\right) \tag{54}$$

in the critical limit ($\mu_2 = \mu_{\text{crit}}$), and bigger angles for $\mu_2 > \mu_{\text{crit}}$; therefore the perturbation does not grow. In contrast, for $\rho < 0$, the vertex A_1 moves away from the y axis, with an initial angle of

$$\varphi = \pi - \tan^{-1}\left(\frac{R}{1+\sqrt{1-R^2}}\right), \tag{D14}$$

which is practically along the butterfly wing. In this case, the junctions separate initially from each other and the butterfly configuration is unstable.

[1] T. W. B. Kibble, J. Phys. A **9**, 1387 (1976).
[2] M. B. Hindmarsh and T. W. B. Kibble, Rep. Prog. Phys. **58**, 477 (1995).
[3] A. Vilenkin and E. P. S. Shellard, *Cosmic Strings and Other Topological Defects* (Cambridge University Press, Cambridge, UK, 1994).
[4] R. Jeannerot, J. Rocher, and M. Sakellariadou, Phys. Rev. D **68**, 103514 (2003).
[5] S. Sarangi and S.-H. H. Tye, Phys. Lett. B **536**, 185 (2002).
[6] N. T. Jones, H. Stoica, and S.-H. H. Tye, Phys. Lett. B **563**, 6 (2003).
[7] G. R. Dvali and S. H. H. Tye, Phys. Lett. B **450**, 72 (1999); C. P. Burgess, M. Majumdar, D. Nolte, F. Quevedo, G. Rajesh, and R. J. Zhang, J. High Energy Phys. 07 (2001) 047; G. R. Dvali, Q. Shafi, and S. Solganik, arXiv:hep-th/0105203
[8] S. Kachru, R. Kallosh, A. Linde, J. M. Maldacena, L. McAllister, and S. P. Trivedi, J. Cosmol. Astropart. Phys. 10 (2003) 013; H. Firouzjahi and S. H. H. Tye, Phys. Lett. B **584**, 147 (2004).
[9] C. P. Burgess, J. M. Cline, H. Stoica, and F. Quevedo, J. High Energy Phys. 09 (2004) 033.
[10] A. Albrecht, R. A. Battye, and J. Robinson, Phys. Rev. Lett. **79**, 4736 (1997).
[11] N. Bevis, M. Hindmarsh, M. Kunz, and J. Urrestilla, Phys. Rev. D **75**, 065015 (2007).
[12] C. Contaldi, M. Hindmarsh, and J. Magueijo, Phys. Rev. Lett. **82**, 679 (1999).
[13] N. Bevis, M. Hindmarsh, M. Kunz, and J. Urrestilla, Phys. Rev. Lett. **100**, 021301 (2008).
[14] A. A. Fraisse, C. Ringeval, D. N. Spergel, and F. R. Bouchet, Phys. Rev. D **78**, 043535 (2008).

[15] L. Pogosian, S. H. Tye, I. Wasserman, and M. Wyman, J. Cosmol. Astropart. Phys. 02 (2009) 013.
[16] M. V. Sazhin, M. Capaccioli, G. Longo, M. Paolillo, and O. S. Khovanskaya, arXiv:astro-ph/0601494.
[17] B. Shlaer and M. Wyman, Phys. Rev. D **72**, 123504 (2005).
[18] K. Kuijken, X. Siemens, and T. Vachaspati, arXiv:0707.2971.
[19] T. Damour and A. Vilenkin, Phys. Rev. Lett. **85**, 3761 (2000); Phys. Rev. D **64**, 064008 (2001); **71**, 063510 (2005).
[20] X. Siemens, V. Mandic, and J. Creighton, Phys. Rev. Lett. **98**, 111101 (2007).
[21] C. J. Hogan, Phys. Rev. D **74**, 043526 (2006).M. R. DePies and C. J. Hogan, Phys. Rev. D **75**, 125006 (2007).
[22] G. Vincent, N. D. Antunes, and M. Hindmarsh, Phys. Rev. Lett. **80**, 2277 (1998).
[23] M. Hindmarsh, S. Stuckey, and N. Bevis, Phys. Rev. D **79**, 123504 (2009).
[24] E. P. S. Shellard, Nucl. Phys. **B283**, 624 (1987).
[25] J. Polchinski, Phys. Lett. B **209**, 252 (1988).
[26] E. J. Copeland and N. Turok, FERMILAB Report No. FERMILAB-PUB-86-127-A, 1986.
[27] E. P. S. Shellard and P. J. Ruback, Phys. Lett. B **209**, 262 (1988).
[28] R. A. Matzner, Comput. Phys., **51** (1988).
[29] M. G. Jackson, N. T. Jones, and J. Polchinski, J. High Energy Phys. 10 (2005) 013.
[30] M. G. Jackson, J. High Energy Phys. 09 (2007) 035.
[31] A. Hanany and K. Hashimoto, J. High Energy Phys. 06 (2005) 021.
[32] A. Avgoustidis and E. P. S. Shellard, Phys. Rev. D **73**, 041301 (2006).
[33] P. M. Saffin, J. High Energy Phys. 09 (2005) 011.
[34] E. J. Copeland, T. W. B. Kibble, and D. A. Steer, Phys. Rev. Lett. **97**, 021602 (2006).
[35] E. J. Copeland, T. W. B. Kibble, and D. A. Steer, Phys. Rev. D **75**, 065024 (2007).
[36] D. Spergel and U. L. Pen, Astrophys. J. **491**, L67 (1997).
[37] P. McGraw, Phys. Rev. D **57**, 3317 (1998).
[38] E. J. Copeland and P. M. Saffin, J. High Energy Phys. 11 (2005) 023.
[39] M. Hindmarsh and P. M. Saffin, J. High Energy Phys. 08 (2006) 066.
[40] A. Rajantie, M. Sakellariadou, and H. Stoica, J. Cosmol. Astropart. Phys. 11 (2007) 021.
[41] J. Urrestilla and A. Vilenkin, J. High Energy Phys. 02 (2008) 037.
[42] L. M. A. Bettencourt and T. W. B. Kibble, Phys. Lett. B **332**, 297 (1994).
[43] N. Bevis and P. M. Saffin, Phys. Rev. D **78**, 023503 (2008).
[44] P. Salmi, A. Achucarro, E. J. Copeland, T. W. B. Kibble, R. de Putter, and D. A. Steer, Phys. Rev. D **77**, 041701 (2008).
[45] E. B. Bogomolny, Yad. Fiz. **24**, 861 (1976) [Sov. J. Nucl. Phys. **24**, 449 (1976)].
[46] Note that a negative ρ corresponds to the arc A_1A_2 in Fig. 7 going from concave, as shown, to convex. Equivalently, the center of the circle from which the arc is formed moves from below the arc, as in the figure, to above it.
[47] E. J. Copeland, R. C. Myers, and J. Polchinski, J. High Energy Phys. 06 (2004) 013.
[48] E. J. Copeland, H. Firouzjahi, T. W. B. Kibble, and D. A. Steer, Phys. Rev. D **77**, 063521 (2008).
[49] K. J. M Moriarty, E. Myers, and C. Rebbi, Phys. Lett. B **207**, 411 (1988).
[50] E. Witten, Phys. Lett. **153B**, 243 (1985).